Volume 4
Number 11
November 2025
Pages 1315–1404

Energy Advances

rsc.li/energy-advances

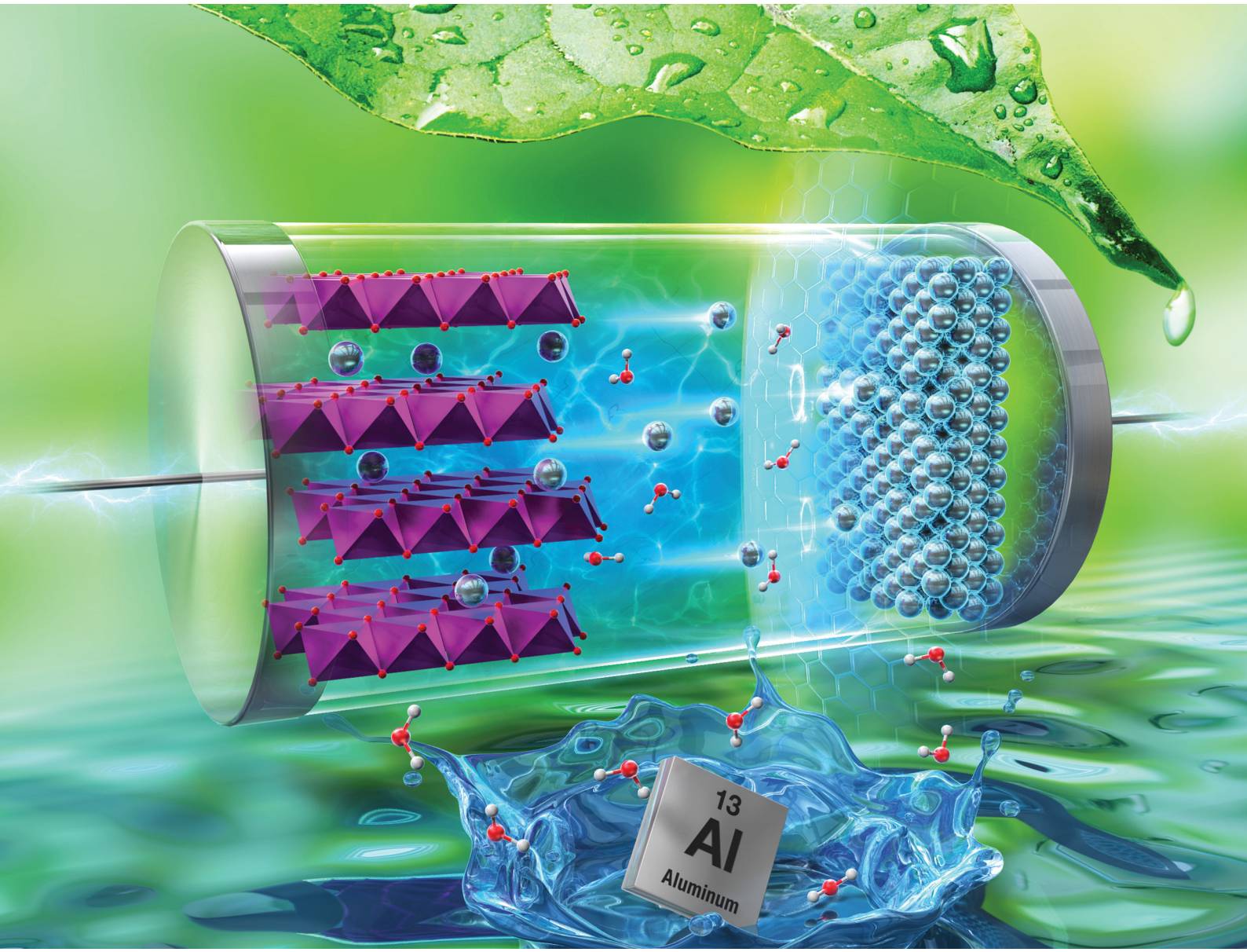

ISSN 2753-1457

ROYAL SOCIETY OF CHEMISTRY

REVIEW ARTICLE
Ryohei Mori
Aqueous rechargeable aluminum battery – a mini review

Energy Advances

ROYAL SOCIETY OF CHEMISTRY

REVIEW ARTICLE

View Article Online
View Journal | View Issue

Cite this: *Energy Adv.*, 2025, 4, 1321

Aqueous rechargeable aluminum battery – a mini review

Ryohei Mori [ab]

Received 30th May 2025,
Accepted 5th August 2025

DOI: 10.1039/d5ya00148j

rsc.li/energy-advances

Recently, rechargeable aqueous aluminum ion batteries (RAAIBs) have been a promising candidate as the next-generation secondary battery in the rechargeable battery industry owing to its enhanced theoretical specific energy, low cost, and environmental friendliness. The manufacturing cost and price of battery components are very low because they can be prepared in ambient atmosphere and have a simple manufacturing process, which is advantageous compared to other battery types. Furthermore, the raw materials that comprise the battery's components are easily available and not expensive. However, currently its inferior cycle stability precludes real industrial application. In this article, the current progress in development of RAAIBs is briefly summarized based on the type of aluminum salt, including aluminum fluoride, chloride, sulfide, nitride, and others. Additionally, research areas necessary for improving the electrochemical performance of RAAIB will be discussed.

1. Introduction

The rechargeable battery is one of the most important electronic devices for renewable energy systems. Currently, the representative rechargeable battery technology is the lithium ion battery, despite lithium's scarcity in some regions of the world and its ever-increasing price.[1] Thus, development of another metal-based rechargeable battery technology is urgently needed. In this regard, aluminum (Al)-based rechargeable batteries are a promising alternative because Al is the third most abundant element on Earth, making Al-based batteries potentially much cheaper than lithium ion batteries. In addition, Al is the most recyclable metal industrially, with a firmly established recycling system.[2] The size of aluminum trivalent ions is small (0.535 Å), which is in theory ideal for creating rechargeable batteries with high energy density.[3–5] An Al-based redox couple, which involves three electron transfers during electrochemical charge/discharge reactions, provides storage capacity surpassing that of the single electron transfer lithium-ion battery. Compared to its monovalent and divalent counterparts, trivalent Al exhibits the highest theoretical charge capacity per unit volume (8046 mAh cm^{-3}), which is approximately four times that of Li (2042 mAh cm^{-3}, Table 1).[6] Although the theoretical gravimetric capacity of Al (2980 mAh g^{-1}) is lower than that of Li (3861 mAh g^{-1}), it is still superior to many other metals. Because of these exceptional characteristics, Al batteries are an attractive candidate for rechargeable batteries in smartphones, computers, electric vehicles (EVs), as well as for smart grids. From an industrial standpoint, large-scale development of Al-based rechargeable batteries offer the possibility of high energy density with low cost, resource stability and safety when coupled with suitable electrolytes and cathode materials.

Large number of research has been studied to develop Al ion batteries (AIBs) and the battery components materials are different from those for lithium ion battery. So far, transition metal oxides such as MnO_2, V_2O_5, TiO_2 and WO_3 *etc.*... have been investigated as cathode material.[7–10] Transition metal sulfides such as MoS_2, Co_3S_4 *etc.*... also have been applied as cathode.[11,12] Prussian blue analog,[13] organic compound,[14] conductive polymer such as polyaniline,[15] and carbon based materials such as graphite,[16] graphene,[17] carbon nanotube[18] also have been studied as candidate cathode materials. Apart from AIBs, sulfur also has been investigated as cathode for aluminium sulfur battery.[19,20] For anode, not to mention aluminum is the typical anode for AIBs. Aluminum alloy also have been intensively studied and Zn, Cu, Ce, and Sn *etc.*... have been carried out to form intermetallic alloy for AIBs anode.[21] Placing a functionalized interfacial layer on the surface of the Al anode is another method to promote stable electrochemical reaction of AIBs. In this regard, amorphous aluminum,[22] amorphous carbon,[23] Mxene[24] *etc.*... were applied as interfacial layer for AIB anode. So far, $AlCl_3$ based electrolyte was especially focused to study for AIBs since $AlCl_3$ demonstrated stable aluminum ion redox reaction. Since $AlCl_3$ possess strong acidity and corrosive nature, molybdenum and niobium were often applied as current collector.[25] Furthermore, in general, glass fiber membranes had been used as separator for AIBs.[26]

[a] *Green Science Alliance Co., Ltd, 2-22-11 Obana, Kawanishi city, Hyogo Prefecture 666-0015, Japan. E-mail: moriryohei@fuji-pigment.co.jp; Fax: +81-72-759-9008; Tel: +81-72-759-8501*

[b] *Fuji Pigment Co., Ltd, 2-23-2 Obana, Kawanishi city, Hyogo Prefecture 666-0015, Japan*

Table 1 Essential properties of various metal anodes applied in metal ion batteries. Gravimetric and volumetric capacity, abundance in Earth's crust, cost, standard potential and cation radius of lithium (Li), sodium (Na), potassium (K), magnesium (Mg), calcium (Ca), and aluminum (Al) are presented

Element	Gravimetric capacity (mAh g^{-1})	Abundance (ppm)	Cost (USD per kg)	Volumetric capacity (mAh cm^{-3})	Standard potential (V *vs.* NHE)	Cation radius (Å)
Na	1166	22 700	3.1	1050	−2.71	1.02
Ca	1340	41 000	2.4	2071	−2.87	1
K	685	18 400	13.1	609	−2.925	1.38
Mg	2205	23 000	2.2	3868	−2.37	0.72
Li	3861	65	19.2	2042	−3.042	0.76
Al	2980	82 000	1.9	8046	−1.66	0.535

In addition, polyacrylonitrile as well as cellulose based separator also have been challenged for AIB separator.[27,28] It should be noted that the standard electrode potential of Al^{3+}/Al is −1.67 V *vs.* SHE.[29] The theoretical energy density for AIBs is 1060 Wh kg^{-1} which is much higher than that of lithium ion battery (406 Wh kg^{-1}).[30] Even though, practical capacity ranges up to a little over 400 Ah Kg^{-1}.[31]

However, certain issues hinder the application of RAAIB. For example, during electrochemical reactions, a thin oxide layer, typically a few nanometer thick, is formed on Al anodes, which behave as a dielectric material (bandgap of 5–8 eV)[32] blocking the reversible plating/stripping reaction. To make use of Al as an anode material, reversible aluminum electrodeposition at high coulombic efficiencies is an essential criterion. This can only be achieved in a limited number of electrolyte systems, particularly those employing Al-halide molten salts, including ionic liquids (ILs) and deep eutectic solvent systems. The first report to overcome this problem used an electrolyte composed of $AlCl_3$ and an IL;[33] since this discovery, considerable numbers of studies using similar electrolyte systems have been reported. It has also been suggested that battery capacity in many RAAIBs originates from monovalent ions ($AlCl_4^-$ and $Al_2Cl_7^-$), which do not fully utilize the advantage of Al's ability to exist as a trivalent ion.[34] Moreover, $AlCl_3$-based IL electrolytes are highly corrosive and sensitive to moisture, making their application in real batteries challenging.[35–42] $AlCl_3$ and IL analogs as deep eutectic solvent-based electrolytes have also been studied for Al-based batteries, although they still possess corrosive characteristics.[43,44] On the other hand, organic electrolytes present an appealing choice for the practical application of rechargeable Al batteries. However, a major challenge that has hindered the development of organic electrolytes for rechargeable Al batteries is the lack of a suitable organic system, as most studies using organic electrolytes do not demonstrate high efficiency for practical usage.[45,46] Finally, solid state electrolyte-based Al batteries have also been studied although high capacity could not be obtained due to high resistance at the electrode/solid electrolyte interface.[47,48]

Based on previous research, it appears aqueous-based electrolytes are still the ideal choice. If Al-based, efficient rechargeable batteries with aqueous electrolytes could be developed, it would make the manufacturing process simpler and cheaper compared to that of the lithium ion battery, because these materials can be prepared in an ambient atmosphere and the need for inert gas such as nitrogen or argon is removed. Al-based batteries can even operate in ambient atmosphere unlike lithium ion batteries, providing an alternative choice for use in industrial rechargeable batteries.

In this review, we will explain the basic principles of Al batteries with aqueous-based electrolyte with a few examples classified by the type of aluminum salt in the aqueous electrolyte. In addition, necessary research directions to improve RAAIBs will be discussed.

2. Metal salts in electrolyte

2.1. Aluminum TFSI and $(OTF)_3$

A major problem in RAAIBs is the formation of oxide layers in Al-based rechargeable batteries. To keep charge conduction and avoid oxide layer formation, potentials that exceed the thermodynamic stability of water is necessary, but would result in undesirable hydrogen evolution reaction (HER), thus the electrochemical window of RAAIBs is constrained. Furthermore, applying Al as an anode for rechargeable battery give rise to more issues, including (i) corrosion, (ii) dendrite formation, and (iii) re-passivation (Fig. 1).[49]

Until now, Al-based metal salts such as $Al(CF_3SO_3)_3$ (also known as $Al(OTF)_3$) have been actively investigated due to the fact that they readily dissociate in water to form hexacoordinated Al-ion complexes.[50] Although aqueous electrolytes typically possess narrow electrochemical stability limited by the electrochemical window (thermodynamically as low as 1.23 V) of water, recent studies demonstrated that aqueous electrolytes can stably operate up to >2 V by incorporating highly concentrated aqueous solutions of metal salts containing perfluorinated anions such as TFSI. Molecular dynamics simulations have elucidated that their stability at a high oxidation state is related to water depleted zone formation at the Al anode surface, owing to the accumulation of TFSI anions.[51] The anion OTF^- participates in the Al^{3+} solvation structure as $[Al(H_2O)_4(OTF)]^{2+}$.[52,53]

Costa *et al.* investigated the influence of $Al(OTF)_3$ concentration in aqueous electrolyte for RAAIB with carbon as the cathode material.[54] As one can see in Fig. 2(a), 5 M of $Al(OTF)_3$ electrolyte results in an unstable charge–discharge profile, with drifting potentials and polarization augmentation (from ~0.7 V at 20 h to 1.0 V at 180 h), likely due to reduced ionic conductivity and increased viscosity.[55] When $Al(OTF)_3$ concentration decreases, polarization values became smaller and

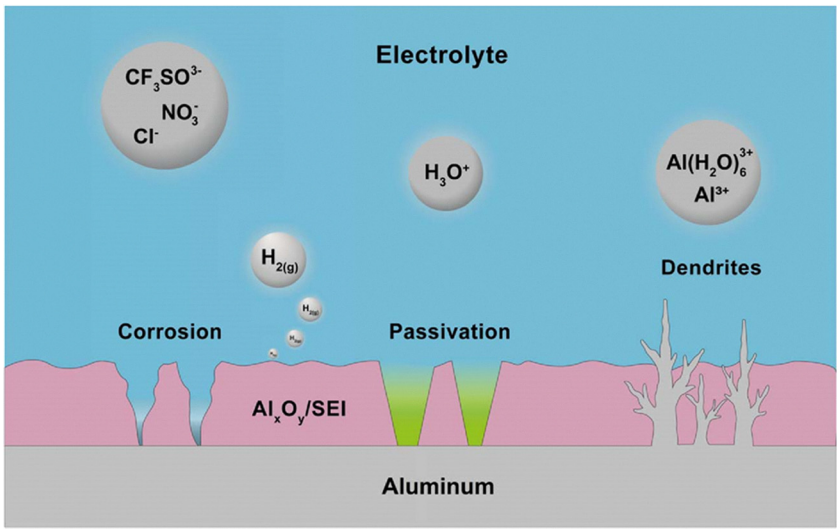

Fig. 1 Obstacles at the aluminum and electrolyte interface: illustrated explanation of possible phenomena and chemical species is shown assuming under water based electrolytes with acidic condition.

charge–discharge curves become more stable. Electrochemical impedance spectroscopy (EIS) was also used to elucidate battery resistance at various reaction times (Fig. 2(b)). Right after the battery has been prepared, inductive loops at low frequencies can be observed, owing to its modification by ion adsorption processes because the boundary between the Al anode and the electrolyte is not well established.[56] Resistance dropped as the electrochemical reaction proceeded over 100 hours (Fig. 2c), and increased again with an additional 100 hours of battery operation (Fig. 2d). From these results, it can be deduced that resistance depends heavily on the concentration of Al salt in the electrolyte and electrochemical reaction time. From their study, $Al(OTF)_3$ at 2 M concentration gave the best results with lowest battery resistance, in good agreement with other reports.[50,56] It should be noted here that surface modification of the Al anode is also a critical factor that was performed in their study.[54] Typical surface modification involves IL treatment of the Al anode, which improves the battery characteristics. We will briefly discuss IL and deep eutectic solvent surface treatment of Al anodes in a later section.

Carbon is a common choice for cathodes in both aqueous and non-aqueous rechargeable Al batteries. Graphite is one of the representative carbon-based materials studied, although their hydrophobicity hinders the access of aqueous electrolyte, resulting in poorer electrochemical performance. To overcome this, graphite modified into reduced graphene oxide (rGO) materials with some hydrophilicity were investigated as a cathode material for aqueous Al ion batteries.[57] Fig. 3(a) presents the Raman spectra of rGO in its charged and discharged states; rGO appears to be relatively stable against charge–discharge reactions since no obvious change was observed for the G-band in terms of its frequency, width, and I_G/I_D (Intensity of G band/D band) values. Presence of the anion OTF^- in the electrolyte was confirmed by 1251, 1033, and 641 cm^{-1} bands in Fourier transform infrared spectroscopy (FTIR) measurements (Fig. 3(b)). In addition, the frequency of the C–O stretching mode was red shifted after discharge due to electronic charge transfer.[58] The C 1s X-ray photoelectron spectroscopy (XPS) results elucidated the presence of C–O, C═O, and O–C═O bonding at 286.0, 287.2, and 288.6 eV, respectively. Moreover, the C–F_x bond arising from $(OTF)_3^-$ can be observed at 292 eV (Fig. 3(c)). The Al 2p XPS spectra presented the binding energy of the Al 2p shell as two peaks, centered at 75.9 eV and 75.0 eV (Fig. 3(d)). The main peak of discharged state is at 75.9 eV, indicating the absence of salt, which can be attributed to the formation of $[Al(H_2O)_6]^{3+}$. The band at 75.0 eV is more dominant for the charged state, suggesting a different chemical environment surrounding Al. The ^{27}Al solid-state nuclear magnetic resonance (SS NMR) analysis suggested that the band originates from dimer $[Al_2(OH)_2(H_2O)_8]^{4+}$ and/or trimer $[Al_3(OH)_4(H_2O)_{10}]^{5+}$.[59] Furthermore, it was elucidated that the band at 72.6 eV attributed to metallic Al was absent, indicating no Al deposition and dendrite formation risk on the cathode. In summary, XPS analysis proved that Al ions migrate to the rGO cathode during discharge.

To further scrutinize Al ion species in the aqueous state, solid-state magic angle spinning (SS-MAS) NMR analysis was performed.[57] In water, the most stable form of Al^{3+} is $[Al(H_2O)_6]^{3+}$. Initially, intact $Al(OTF)_3$ was measured with NMR under Ar atmosphere to compare against $Al(OTF)_3$ exposed to moisture over various durations, as $Al(OTF)_3$ is extremely hygroscopic. The ^{27}Al spectrum of pure $Al(OTF)_3$ presented a clear resonance at −8.3 ppm (Fig. 4a). When $Al(OTF)_3$ was solvated in water by exposure to ambient atmosphere for 30 min, another weak signal at 1.2 ppm was observed. When $Al(OTF)_3$ was exposed to ambient atmosphere for 1 day, a significant peak at 1.4 ppm emerged. Simultaneously, the peak at −8.3 ppm shifted by 0.2 ppm and its intensity was attenuated. These changes are likely due to newly formed species $[[Al(OH)_n(H_2O)_{6-n}]^{(3-n)+}]$ (where n = 0–2). It was suggested that the 1.4 ppm signal is characteristic of the

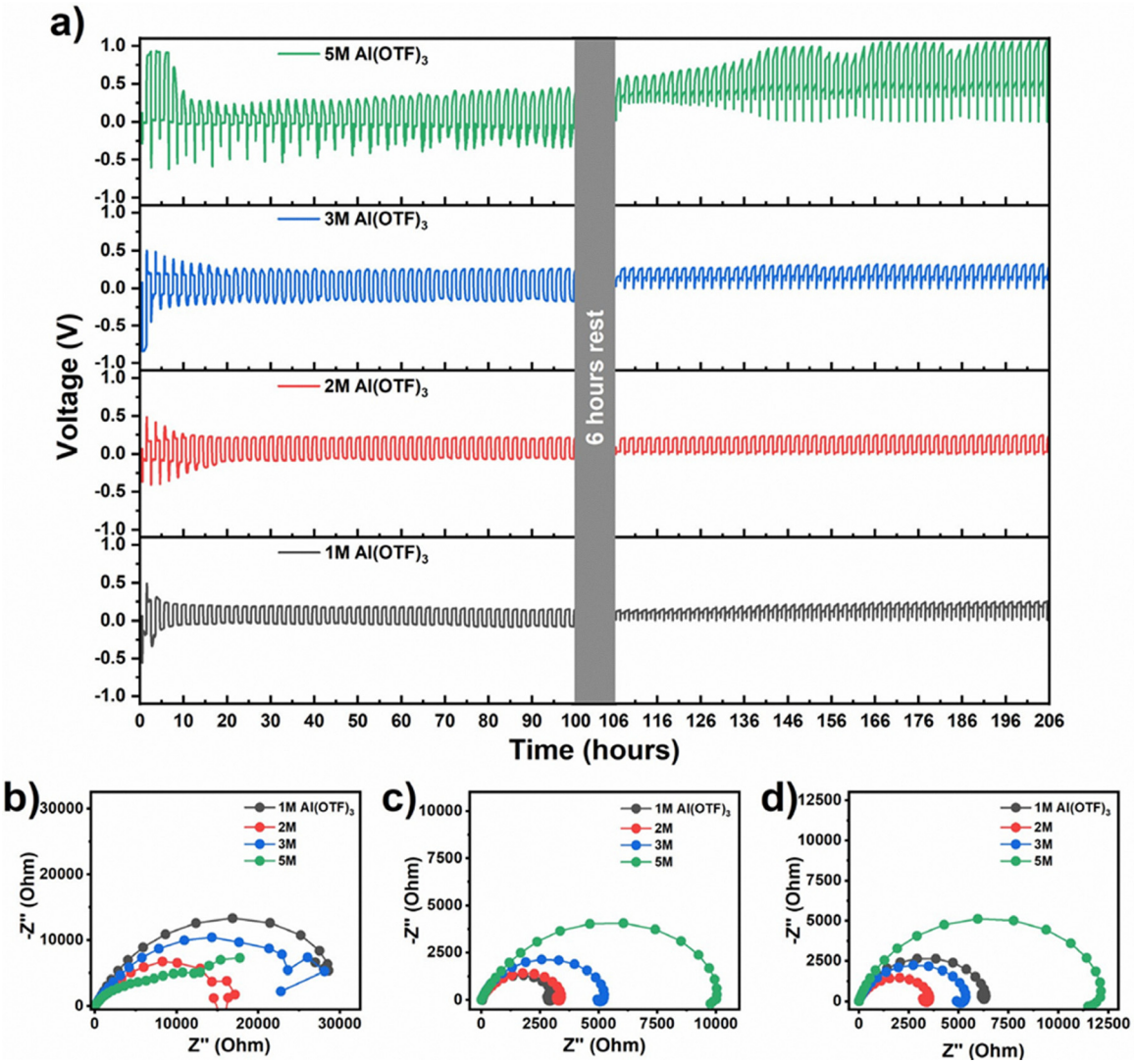

Fig. 2 (a) Stability of the electrolyte under charge–discharge current of ±0.01 mA cm^{-2}. (b) Electrochemical impedance spectroscopy (EIS) of the electrolyte before electrochemical reaction. (c) EIS of the electrolyte after 100 h of electrochemical reaction. (d) EIS of the electrolyte after 200 h of electrochemical reaction.

most stable species, $[Al(H_2O)_6]^{3+}$, whereas the −8.3 ppm peak originated from Al hexa-coordinated oxygen donor ligands.[60] ^{1}H SS-MAS NMR was performed for further confirmation (Fig. 4b). It was interesting to see signals from intact $Al(OTF)_3$ because hydrogen is not contained in the chemical formula. A broad peak at 0–15 ppm and two prominent peaks at 5.0 and 7.2 ppm were observed. This was ascribed to residual water and OTF from the synthesis procedure of $Al(OTF)_3$. As solvation proceeded, bands became narrower and both peaks were shifted. At this stage, different complexes of (semi-) hydrated aluminum or hydronium species (H_3O^+) can be assigned. After 24 hours, one clear peak emerged at 6.0 ppm, which originates from $[[Al(OH)_n(H_2O)_{6-n}]^{(3-n)+}]$ (where n = 0–2) as similarly observed in the ^{27}Al NMR measurement. NMR measurement was also performed on the rGO cathode (Fig. 4c). Before any electrochemical reaction, no peaks were observed in the ^{27}Al NMR measurement for the rGO cathode, confirming no elemental traces of Al on the cathode before any electrochemical reaction. After a charge and discharge sequence, peaks and shoulders at 1.8 and 6.4 ppm were observed. Similarly to Fig. 4(a), peaks at 1.8 ppm can be attributed to the monomer $[Al(H_2O)_6]^{3+}$, while shoulders at 6.4 ppm are attributed to the formation of dimers and/or trimers of the type $[Al_2(OH)_2(H_2O)_8]^{4+}$ and $[Al_3(OH)_4(H_2O)_{10}]^{5+}$.[61]

^{1}H NMR spectra demonstrated that the rGO cathode had a broad band extending from −10 to 20 ppm centered at 6.3 ppm, confirming that the rGO cathode contains functional groups such as hydroxyls and carboxyls, as well as bound water retained from the freeze dry process in rGO cathode preparation. Peaks at 2.1 ppm were detected for all intact and electrochemically cycled rGO samples and are suggested to originate from aliphatic carbons at the edge of the graphene basal planes. Furthermore, the 4.4 ppm peak

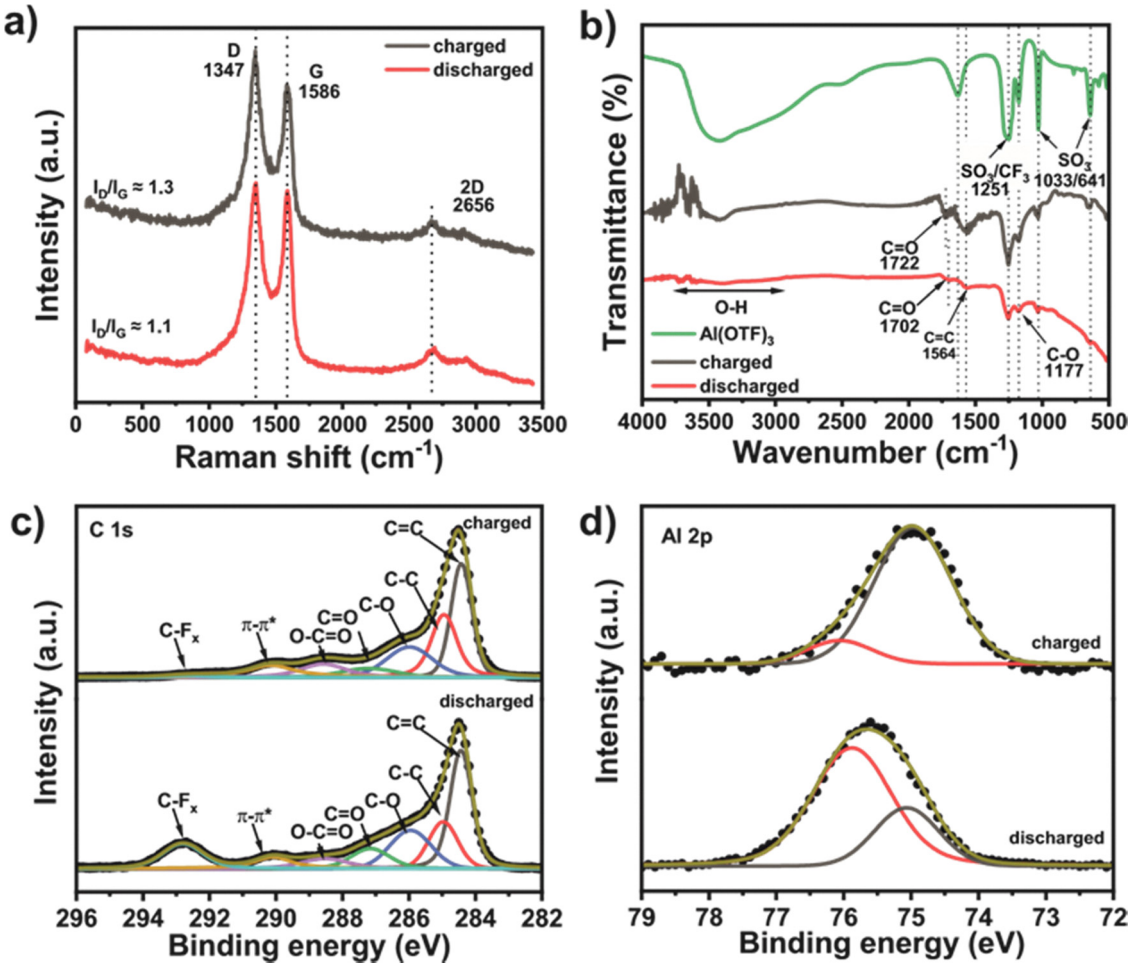

Fig. 3 Spectra of rGO cathodes at charged and discharged condition. (a) Raman spectroscopy. (b) FTIR. (c) C 1s XPS. (d) Al 2p XPS. All spectra are normalized by the highest intensity.

corresponds to the protons in the solvated Al monomer, $[Al(H_2O)_6]^{3+}$.

So far, we have investigated the details of $Al(OTF)_3$ solvation during RAAIB operation. This leads to discussion of studies to improve battery performance with various electrolyte mixtures. Li *et al.* prepared mixed electrolyte composed of 5 M $Al(OTF)_3$ and 0.5 M LiOTF for an aqueous Al battery,[62] which was able to reduce corrosion caused by hydrogen evolution. When LiOTF was added to $Al(OTF)_3$, the solvation sphere of Al^{3+} changes from a fully octahedral structure to partly tetrahedral and octahedral, decreasing the complexes' hydrogen bonding toward water molecules, which reduces hydrogen evolution. As a result, the stability of the electrochemical window was improved to 3.8 V, with an initial charge capacity of 437 mAh g^{-1} and 103 mAh g^{-1} after 100 cycles.

Ran *et al.* attempted to use Al-based alloys for Al aqueous rechargeable batteries.[63] They prepared lamella-nanostructured eutectic $Al_{82}Cu_{18}$ alloy anodes, improving electrochemical stability by preventing Al dendrite growth during stripping/plating cycles. $AlxMnO_2$ was used for the cathode and the prepared battery demonstrated stable Al stripping/plating for 2000 h with an overpotential smaller than ±53 mV. The initial discharge capacity was ~400 mAh g^{-1} and 83% capacity was maintained after 400 cycles. This improvement was achieved based on utilizing the difference in corrosion potential between α-Al lamellas and Al_2Cu lamellas to obtain low overpotentials, in which α-Al transferred Al^{3+} charge carriers to Al_2Cu.

Other studies have focused on cathode materials. Wu *et al.* used $Al_xMnO_2{\cdot}nH_2O$ synthesized by an *in situ* electrochemical transformation reaction as a cathode material with $Al(OTF)_3$–H_2O electrolyte, which exhibited high specific capacity and energy density of 467 mAh g^{-1} and 481 Wh kg^{-1}, respectively. To scrutinize the origin of this high performance, combined experiments with different conditions were performed with spinel Mn_3O_4 or $Al_xMnO_2{\cdot}nH_2O$ as cathodes, and the three different types of electrolyte: $Al(OTF)_3$–H_2O, HOTF (triflic acid), and $AlCl_3$/[BMIM]Cl.[64] The HOTF-based electrolyte was examined to clarify the effect of Al^{3+}, and $AlCl_3$/[BMIM]Cl was applied as a comparison to an IL-based electrolyte. In addition, to examine the possibility of H_3O^+ influencing the RAAIB capacity, coin cell structures of carbon fiber paper (CFP)/HOTF–H_2O/Mn_3O_4 and CFP/HOTF–H_2O/$Al_xMnO_2{\cdot}nH_2O$ were prepared (Fig. 5(a)). The concentration of H_3O^+ was adjusted to be the same as $Al(OTF)_3$–H_2O based electrolyte a precise

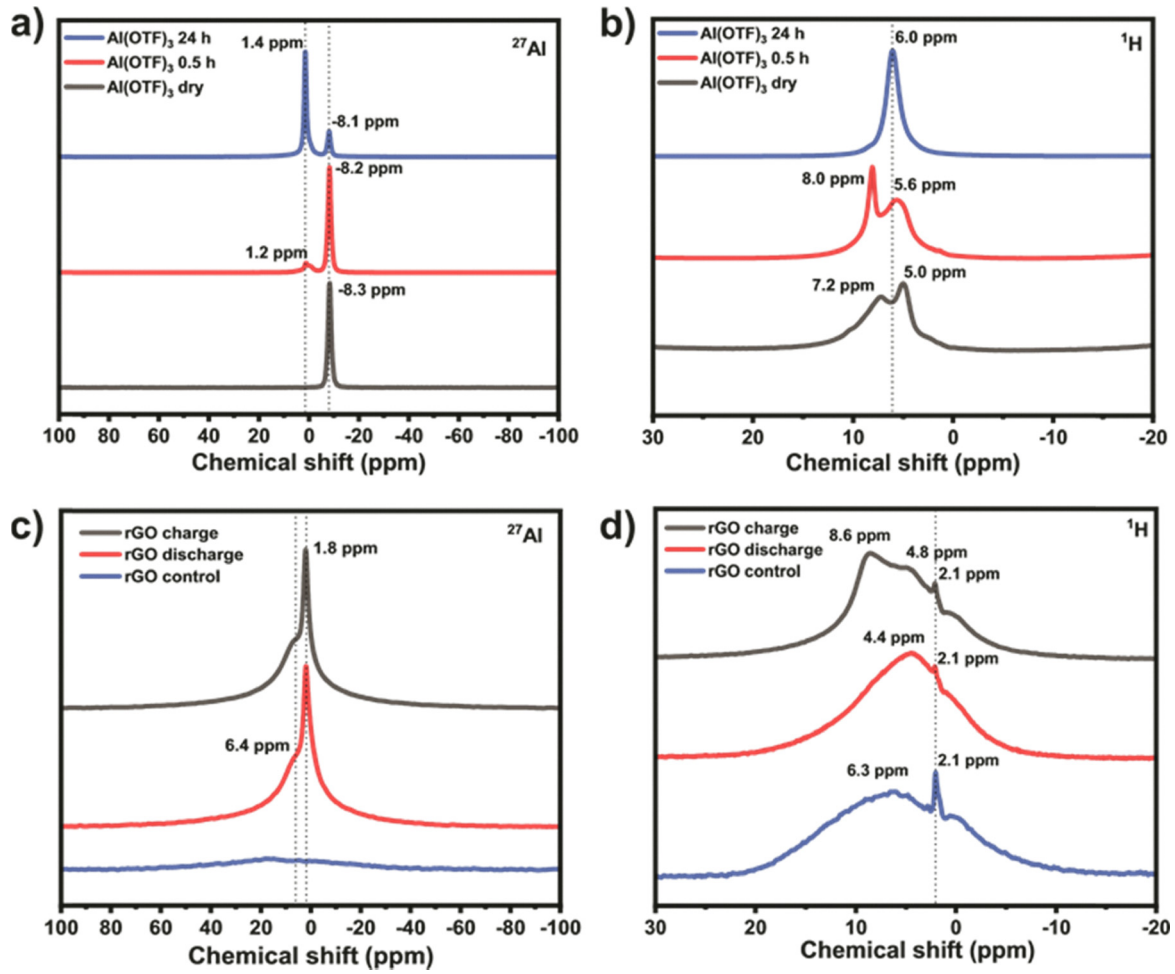

Fig. 4 SS MAS A(Solid State Magic Angle Spinning) NMR spectra offal($OTF)_3$, freeze dried and the cycled rGO cathodes. (a) ^{27}Al spectra of the Al$(OTF)_3$ salt. (b) ^{1}H spectra of the Al$(OTF)_3$ salt. (c) ^{27}Al spectra of the rGO at each condition. (d) ^{1}H spectra of the rGO at each condition.

comparison. Fig. 5b–d show that both CFP/HOTF–H_2O/Mn_3O_4 and CFP/HOTF–H_2O/$Al_xMnO_2{\cdot}nH_2O$ exhibited no discharge capacity, implying that all discharge capacity arose from Al^{3+} intercalation and H_3O^+ does not contribute to electrochemical performance at all.

2.2. Aluminum chloride

Aluminum chloride ($AlCl_3$) is often used as an aluminum salt for IL-based electrolytes, although they suffer from high material costs as ILs are expensive in general. In this regard, some research based on aqueous electrolytes with $AlCl_3$ have been performed. Das *et al.* had demonstrated that graphite is capable of reversibly hosting Al^{3+} ions and was combined with TiO_2 in 1 M of $AlCl_3$ aqueous electrolyte (Fig. 6(a and b)).[65] The battery demonstrated an average discharge voltage of 1.5 V with over 1000 cycles of charge–discharge stability. Cyclic voltammetry data of the prepared Al-ion battery is shown in Fig. 6(c), showing a pair of cathodic and anodic redox peaks (indicated as A and B) at 0.4 and 0.5 V (*vs.* Ag/AgCl), respectively. Moreover, Fig. 6(d) shows the charge–discharge curve at an applied current of 0.05 mA cm^{-2}, where a very small charge–discharge plateau at approximately 0.5 and 0.4 V (*vs.* Ag/AgCl), coinciding with the results of cyclic voltammetry, can be observed.

Since $AlCl_3$ is strongly corrosive, Cakan *et al.* investigated the influence of current collectors on the Al-ion battery with 1.0 M of $AlCl_3$ aqueous electrolyte. Four types of current collectors, namely nickel foil, titanium foil, graphite plate, and stainless steel, were examined and corrosion tests, charge–discharge, and cyclic voltammetry measurements were performed.[66] Results indicate graphite as the optimal choice to minimize corrosion and HER. The anatase phase TiO_2 was applied as the cathode material with graphite plate, yielding initial discharge capacity of 249 mAh g^{-1} at a current density of 3 A g^{-1}.

Besides aluminum, other elements were used in a metal salt for Al-ion battery electrolytes. Tao *et al.* added iron to $AlCl_3$-based electrolyte to form a hydrolyzed, polymerized Al–Fe hybrid electrolyte (poly aluminum ferric chloride, PAFC), which enhanced electrochemical performance.[67] The prepared electrolyte contributes to the capacity through an iron redox reaction, proceeding in parallel with aluminum redox when an Al–Fe alloy was used as an anode. This type of hybrid Al–Fe ion battery demonstrated 35 Ah L^{-1} under 1.0 mA cm^{-1} of current density with 90% capacity retention after 500 cycles.

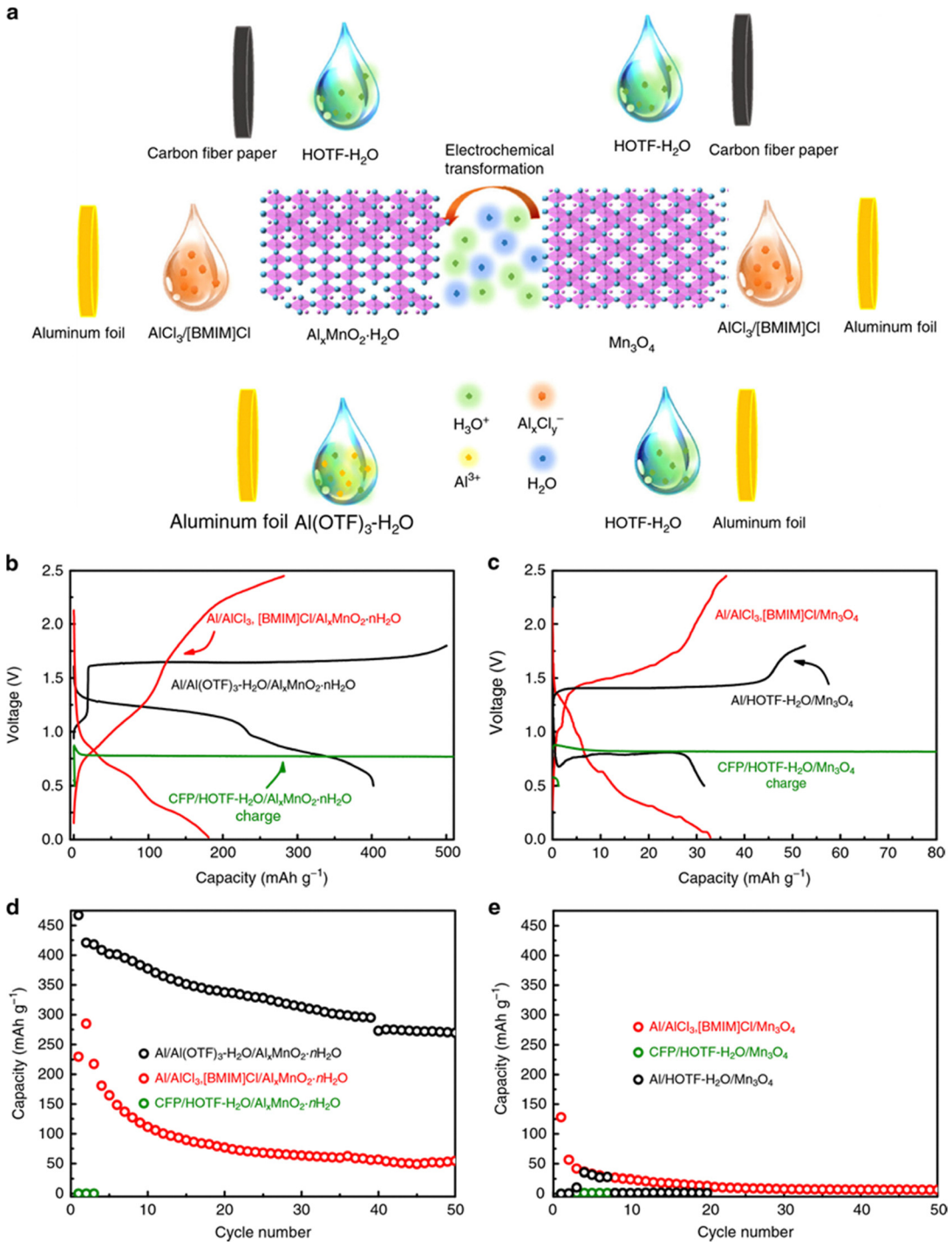

Fig. 5 The schematic figure of each experiments. (a) Experiment is performed with $Al_xMnO_2{\cdot}nH_2O$ cathode and Mn_3O_4 anode with aqueous and ionic liquid electrolytes. (b) and (d) Charge and discharge curves at each experimental condition. (c) and (e) Discharge capacity t each experimental condition.

This special hydrolyzed PAFC was synthesized by the polymerization reaction of aluminum chloride and iron chloride and applied as an electrolyte. To investigate this hybrid metal redox reaction mechanism, FTIR and *ex situ* Raman spectra of the electrolyte were measured and analyzed. The electrolyte specimens were collected at different stages of the electrochemical reaction as exhibited in the time–voltage curve (Fig. 7(a)). The peak at 314 cm^{-1} in the Raman spectra is attributed to Fe ions in Fig. 7(b).[68] The narrow blue zone in Fig. 7(b) was expanded for easy recognition of peak change as presented in Fig. 7(c). The peak decreased as the discharge reaction proceeds from 0.9 to 0.2 V, implying reduction of ferric ions into ferrous ions. On the other hand, from 1.10 to 1.65 V during the charging process, the peak profile was similar to that of open-circuit

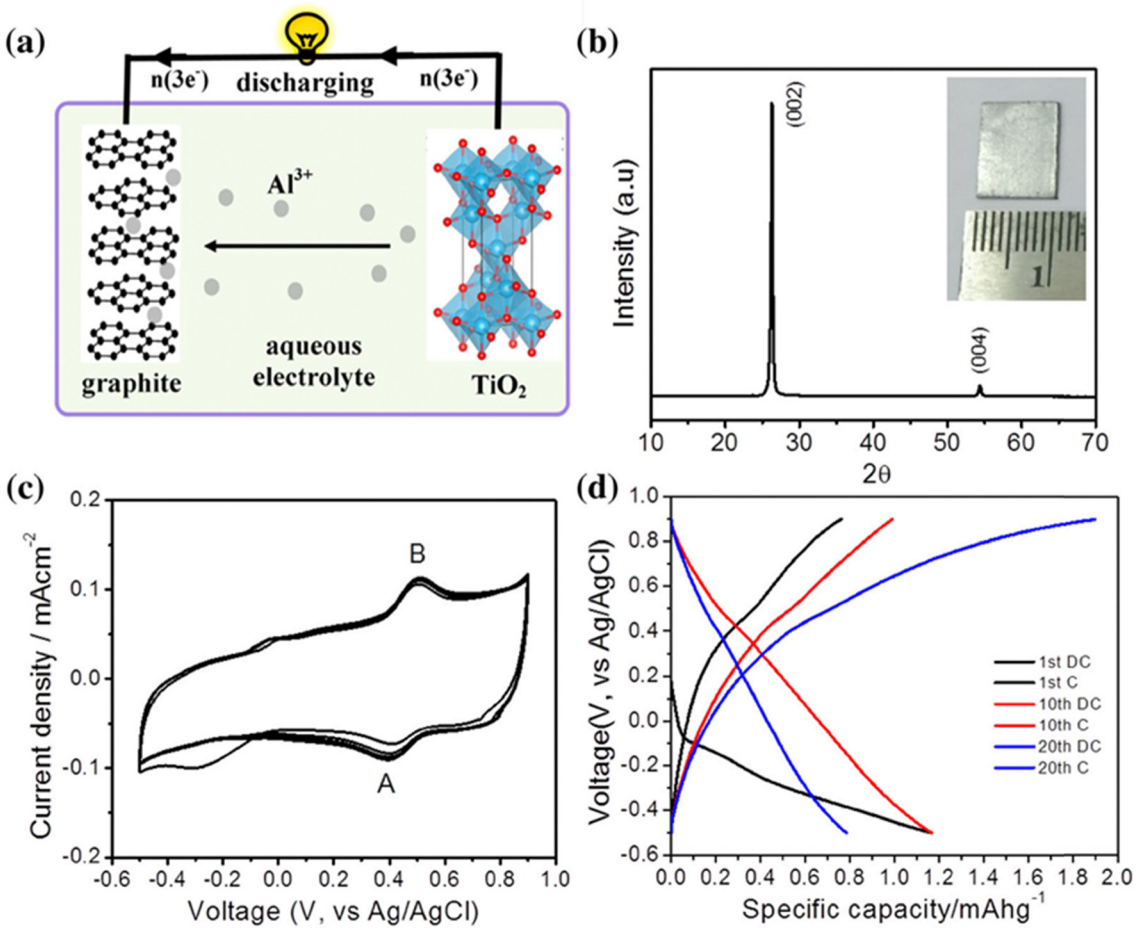

Fig. 6 (a) Schematic image of an aqueous aluminum ion battery with graphite as the cathode and TiO_2 as the anode. (b) XRD pattern of graphite cathode. (c) Cyclic voltammetry at a scan rate of 2.5 mV s^{-1}. (d) Charge–discharge curves of the graphite cathode in a 1 M $AlCl_3$ aqueous electrolyte at a specific current of 0.05 mA cm^{-2}.

voltage state. This phenomenon proves that oxidation/reduction of iron ions is highly reversible, which is the main reason for strong electrochemical performance. Fig. 7(d) is the *ex situ* FTIR spectra of the prepared electrolyte. Peaks at approximately 1610–1630 cm^{-1} are due to H–OH bonding, shifting to frequencies of 590–601 cm^{-1} and 3460–3490 cm^{-1}, indicating the polymerization of hydroxyl aluminum and hydroxyl iron. This study also paved the way for developing high performance Al-ion batteries by applying hybrid-ion electrolytes.

Wills *et al.* prepared an Al-ion battery with CuHCF (copper-hexacyanoferrate) as the positive electrode and TiO_2 as the negative electrode.[69] The electrolyte was composed of 1 M of $AlCl_3$ and KCl. Galvanostatic and cyclic voltammetry analysis revealed that battery capacity was approximately 10 mAh g^{-1} with an average discharge voltage of approximately 1.5 V. Interestingly, the electrode was dark blue–grey in the charged state when observing the TiO_2 on Al anode; this subsequently reverts to the original white color of TiO_2 in the discharged state. It was suggested that the TiO_2 color variation could be ascribed to the reduction of Ti^{4+} to Ti^{3+}, driven by possible reactions of Al^{3+} intercalation, Al^{3+} surface adsorption, or H^+ intercalation and H^+ surface adsorption.

Rastabi *et al.* investigated the metallurgical Al anode behavior in a water-in-salt electrolyte.[70] $AlCl_3{\cdot}6H_2O$ was applied as the metal salt for an aqueous electrolyte and graphite was used as the cathode. The capacity decay from charge–discharge cycling was found to be due to the formation of a detrimental solid–electrolyte interphase (SEI) layer on the Al anode surface. Detailed observation clarified that Al corrosion initiates around the Al_3Fe intermetallic phase, as Al_3Fe particles allow the electrolyte to break the oxide barrier and penetrate into bulk Al. The Al–Fe phase diagram indicates that iron is a normal impurity element for Al and its solubility is less than 0.05%, often resulting in iron-containing intermetallic phases, such as Al_3Fe.[71,72] It should be noted that such impurity precipitation is extremely difficult to eliminate and Al_3Fe exists even in Al that is over 99.9% pure. In addition, the cost of extremely high purity Al of over 99.99% is considerably more expensive and not realistic for application in Al-ion batteries for industries.[73] This study demonstrates that metallurgical study of Al anodes is also important for creating feasible options for aqueous Al-ion batteries.

Xu *et al.* prepared an RAAIB with the MnO_2 cathode with good cycling properties, optimizing Al^{3+} solvation structures

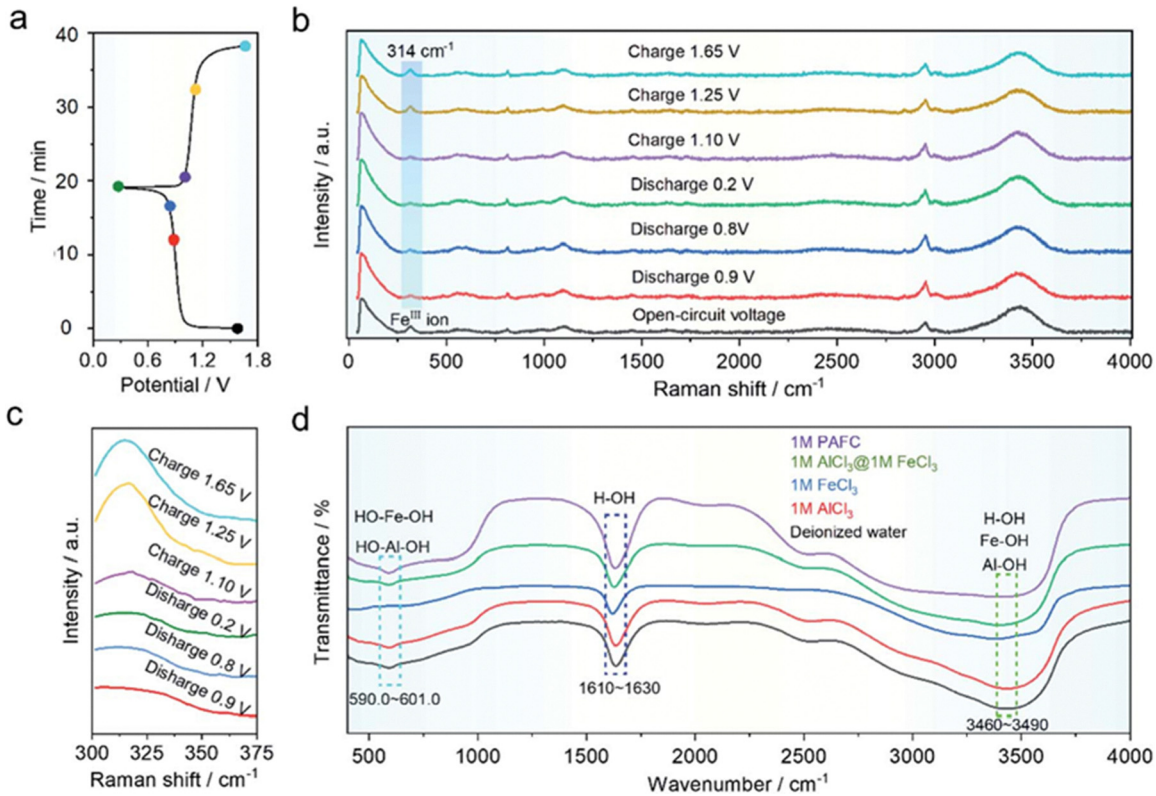

Fig. 7 *Ex situ* electrochemical measurements of PAFC electrolyte at different charge–discharge stages. (a) Potential–time curve during redox reaction. (b) Raman spectra of the electrolyte at respective charge and discharge voltage conditions. (c) Magnified Raman spectra of the blue zone. (d) FT-IR spectra of various electrolyte including PAFC.

by changing electrolyte concentration to prevent Al^{3+} intercalation.[74] By combining molecular dynamics simulations with results obtained from experimental analysis, it was found that the solvation size of Al^{3+} in relatively concentrated electrolyte is wider than MnO_2 lattice spacing, suggesting that Al^{3+} cannot enter into the MnO_2 cathode material (Fig. 8). Namely, the solvation structure and the size of Al^{3+} cations are larger in the preferably modified saturated electrolyte (s-Al/Mn electrolyte composed of 4.4 M $AlCl_3$ and 1 M $MnCl_2$ in H_2O) than in the diluted electrolyte (d-Al/Mn electrolyte composed of 1 M $AlCl_3$ and 1 M $MnCl_2$ in H_2O). As a result, self-intercalation with the MnO_2 cathode lattice could be suppressed due to the larger size of Al^{3+} in the optimized saturated electrolyte. Owing to this optimized electrolyte concentration effect, prepared RAAIBs achieved a specific capacity of ~493 mAh g^{-1} over 1000 cycles.

With respect to chloride-based Al complex metal salts, $Al(ClO_4)_3{\cdot}9H_2O$ has been attempted in electrolytes for Al ion batteries. Even though $Al(ClO_4)_3{\cdot}9H_2O$ is a chloride-based Al complex, its non-corrosive characteristics compared to $AlCl_3$ is the big advantage for industrial application.[75] It should be noted that $Al(ClO_4)_3{\cdot}9H_2O$ was combined with succinonitrile to form a hydrated eutectic electrolyte and not an aqueous one. Author's group also have applied $Al(ClO_4)_3{\cdot}9H_2O$ as the metal salt in the electrolyte and successfully prepared an Al ion battery.[76,77]

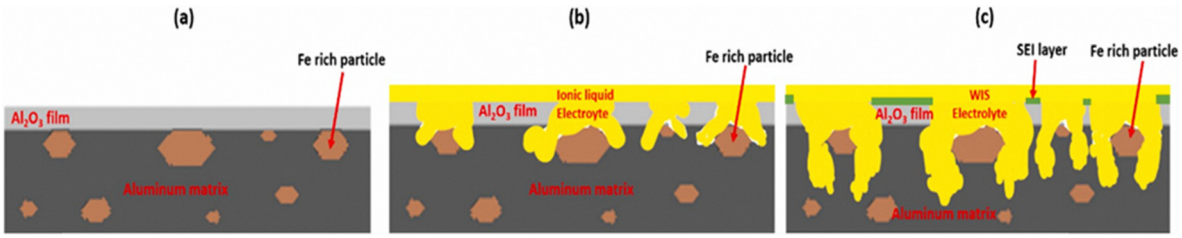

Fig. 8 Schematic image presenting Al anode corrosion as electrochemical reaction proceeds. (a) Intact Al anode. (b) After contacting with ionic liquid based electrolyte. One can observe the corrosion around Al_3Fe particles. (c) After contacting with aqueous based electrolyte. One can observe the corrosion around Al_3Fe particles and solid electrolyte interface layer is formed on unbroken oxide film.

2.3. Aluminum nitride, sulfide

There have been some attempts to apply $Al(NO_3)_3$ as a metal salt in electrolytes for Al ion batteries. Nanocubic structured potassium cobalt hexacyanoferrate ($K_2CoFe(CN)_6$) synthesized by a hydrothermal method was used as a cathode successfully in an RAAIB with a capacity of 50 mAh g^{-1} at 0.1 A g^{-1} with 1 M of $Al(NO_3)_3$ as an electrolyte.[78] Wang *et al.* had prepared a flexible RAAIB with a MoO_3 anode coated with polypyrrole (PPy) and a copper hexacyanoferrate cathode, with 1 M $Al(NO_3)_3$ as an electrolyte. The prepared cell demonstrated high stability with capacity retention of 83.2% for 100 cycles, due to high conductivity from deposited PPy on MoO_3. This battery demonstrated good safety and flexibility because a separator material composed of a PVA–$Al(NO_3)_3$ gel polymer was used. Thus, the battery exhibited high durability against various mechanical stress forces and deformation such as folding, bending, squeezing, twisting, and drilling, which paves the way for application of flexible Al-ion batteries in wearable electronic devices.[79] Lahan *et al.* also applied MoO_3 to prepare an aqueous Al-ion battery to examine wether Al^{3+} ions intercalate into MoO_3 in aqueous-based electrolytes.[80] It was confirmed that $AlCl_3$ aqueous electrolyte demonstrated better electrochemical performance than $Al_2(SO_4)_3$ and $Al(NO_3)_3$ aqueous electrolytes due to factors such as higher storage capacity of Al^{3+} ions, retention of battery capacity, and long-term stability. Wu *et al.* studied the influence of IL surface modification and Al alloying (Al–Cu alloy or Zn–Al alloy) in an aqueous electrolyte with 1 M of $Al(OTF)_3$, $AlCl_3$, and $Al(NO_3)_3$. They observed gas evolution and corrosion during the electrochemical redox process. The anode activity of the aluminum and the surface treated aluminum with IL was mainly evoked by chloride anions or solid–electrolyte interface layer residue. It was also found that when an Al–Cu alloy was applied as an anode, nanolamellar Al_2Cu worked as the catalyst and maintained hydrogen generation. They also confirmed that this gas evolution effect was even more pronounced in the case of a Zn–Al alloy anode.[81]

$Al_2(SO_4)_3$ was applied as an electrolyte and the electrochemical performance was compared to an aluminum bis-(trifluoromethanesulfonyl)-imide ($Al[TFSI]_3$) electrolyte. The Zn-supported Al alloy was used as an anode and MnO_2 as the cathode. The Zn–Al alloy reduces the detrimental effect of surface passivation, which contributed to accelerating Al^{3+}/Al redox reaction.[82] Furthermore, electrodeposited substances on the Zn–Al alloy were mainly composed of uniform nanostructures that tend not to form dendrites, which contributed to excellent cycle performance. However, $Al[TFSI]_3$ exhibited an overall better electrochemical performance compared to the $Al_2(SO_4)_3$-based electrolyte.[82]

Zhao *et al.* had reported that certain types of IL treatment on Al anodes formed SEI, which effectively improved electrochemical performance in aqueous electrolyte. MnO_2 was used as a cathode and the prepared Al-ion battery demonstrated specific energy of approximately 500 Wh kg^{-1}.[83] The composition and structure of SEI formed by $AlCl_3$-based IL electrolyte were investigated. Fig. 9(a) shows the result of the total reflection ATR-FTIR data of $AlCl_3$-based IL electrolyte-treated electrode (TAI electrode). The presence of a few organic functional groups can be observed. C═H groups were confirmed in the pristine ionic liquid, as well as additional C═O groups and the enhancement of the C═C functional group in the TAI electrode. It should be noted here that infrared vibration modes that arise from the imidazolium ring (1100–600 cm^{-1}) in the IL disappeared after IL treatment, proving that imidazolium was incorporated into SEI composition. Fig. 9(b–d) presents the XPS spectra of Al, TAI, and pure Al, where an obvious peak originates from Al_2O_3. On the other hand, the Al2p spectra of the TAl substrate shifted towards higher binding energy, which can be ascribed to Al salt, such as $AlCl_3$. Cl2p XPS spectra also support that the 199 eV peak is consistent with a valence of −1 (Fig. 9(c)). The N1s spectra imply that an abundance of nitrogen-containing species exist in the TAI electrode and the 401 eV peak is ascribed to imidazole ions (Fig. 9(d)). Morphology data revealed that surface topography of the TAI electrode is smoother than that of the pure Al surface (Fig. 9(e and f)). The scanning electron microscopy (SEM) cross-section view clearly shows an interfacial layer that is composed of Al, Cl, and N (Fig. 9(g)). It was also demonstrated that even though the aqueous $Al(OTF)_3)_3$-based electrolyte demonstrated better electrochemical performance, the $Al_2(SO_4)_3$ aqueous electrolyte showed rechargeable performance after IL treatment of the Al anode.

Furthermore, Chunshuang *et al.* succeeded in shifting the reduction potential for aluminum deposition by applying amorphous aluminum anode. It was found that the amorphous structure decreased the nucleation energy barrier of aluminum anode which accelerated the interfacial ion transfer kinetics and obtained enhanced aluminum plating/stripping reaction with $Al_2(SO_4)_3$ electrolyte.[84]

2.4. Aluminum iodide, bromide and aluminum PF_6, BF_4

To the best of our knowledge, there is not much research on RAAIB using aluminum iodide, bromide, PF_6, or BF_4. Instead of utilizing iodide-based electrolyte, iodine-containing nitrogen-doped microporous carbon polyhedrons have been used as an electrode. The prepared Al-ion battery exhibited high specific capacity and high rate performance of 102.6 mAh g^{-1} at 8 A g^{-1}, with good cycling stability. LiTFSI- and $AlCl_3$-based aqueous electrolytes were used, although iodide from the cathode participated in the reversible redox reaction between I_2 and I^-, with $I_3^-$and I_5^- as intermediates.[85] Tian *et al.* also applied iodide as a cathode material by combining it with PVP, conductive carbon, and polytetrafluoroethylene as the binder, with the prepared battery demonstrating a high capacity of over 200 mAh g^{-1} at 0.2C based on I^{3-}/I^- redox chemistry.[86]

Although not a water-based electrolyte, the electrochemical reaction of Al^{3+}/Al was examined in $AlBr_3$ dissolved in ethylbenzene for rechargeable Al ion batteries. It was found that KBr was necessary as an additive to promote Al deposition/dissolution reactions on glassy carbon and platinum electrodes.[87]

Another example of a non-aqueous electrolyte uses ($Al(PF_6)_3$) dissolved in dimethyl sulfoxide (DMSO) to investigate aluminum deposition and reversibility. Al deposition-stripping was

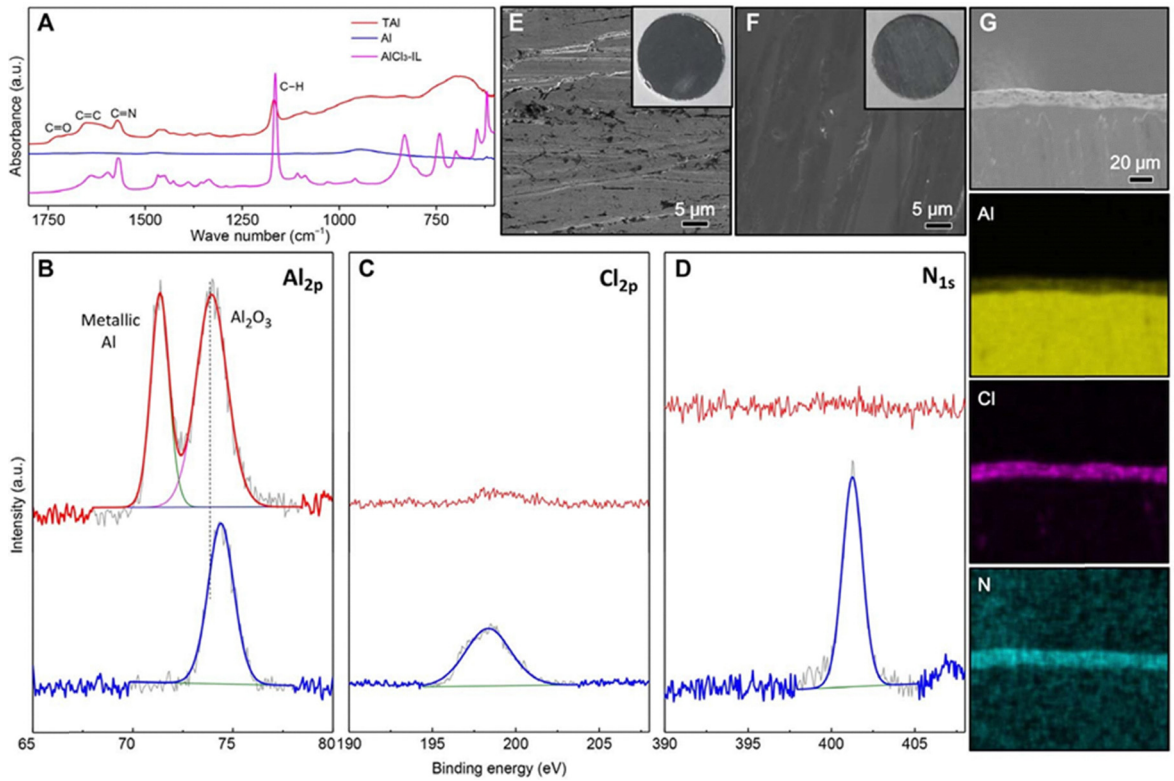

Fig. 9 Surface analysis of metal Al anode before and after treatment with $AlCl_3$-IL electrolyte. (A) ATR-FTIR spectra of Al and TAl surface. XPS spectra of (B) Al 2p (C) Cl 2p (D) N 1s on Al anode (red line) and TAl anode (blue line). SEM pictures of (E) Al anode (F) TAl anode. The insets of (E) and (F) are digital image of Al and TAl (G) Cross-sectional SEM picture of TAl anode and corresponding EDX mapping of Al, Cl, and N. Al: Intact Al anode, TAl: Al anode surface treated with ionic liquid based electrolyte. a.u., arbitrary units.

confirmed with SEM and XPS with depth profiling analysis.[88] The redox reaction was further accelerated by addition of Et_3Al. It was found that continuous cathodic decomposition of DMSO resulted in Al_2O_3 formation on the electrode surface. To the best of our knowledge, there is no studies on RAAIBs using tetrafluoroborate (BF_4)-based electrolytes.

3. Critical research areas

Having discussed above, there still are many issues such as charge–discharge cycling stability that need to be solved before RAAIBs can be applied industrially. At least cycling stability needs to be maintained for over 200 cycles for drones and over 3000 cycles for EV for example.

It seems that fluoride- or chloride-based aqueous electrolytes demonstrate better electrochemical performance overall compared to other types of electrolytes (Table 2). Some research challenges have been explained above although the following are some necessary research topics that need to be investigated to make RAAIB technology feasible.

3.1. Electrolyte mixture. Water base + solvent, alcohol, ionic liquid

Electrolyte composition and utilization of additives in water-based electrolytes is one of the strategies that can improve the electrochemical performance of RAAIBs.

Lahiri *et al.* studied how the addition of ILs to water-based electrolytes influences Al solvation dynamics by density functional theory (DFT) simulations as well as by experiments.[89] DFT calculations elucidated that the coordination number of solvated Al in aqueous ($Al(TfO)_3$) electrolytes could be lowered by adding 1-ethyl-3-methylimidazolium trifluoromethylsulfonate (EMIMTfO), which would result in change of the Al deposition/stripping behavior on the Zn/Al alloy anode. Interestingly, IL addition reduces strain on the manganese oxide cathode during intercalation/deintercalation reactions, which also contributed to better electrochemical performance. FTIR spectroscopy in Fig. 10(a and b) indicates that IL addition induced a shift of CF_3 vibration to lower wavenumbers, which could be related to the change in Al coordination. In the range of between 2000 and 3600 cm^{-1} as presented in Fig. 10(c), additional peaks originating from the imidazolium cation were observed when ionic liquids are introduced.[90] To further investigate the influence of EMIM + TfO^- ions' addition to aqueous electrolytes, DFT-based quantum chemical calculations were performed. Payard *et al.* had previously showed that TfO^- ions would have monodentate or bidentate coordination with Al^{3+} ions.[91] Other DFT calculations and experimental studies also report that six water molecules exist in proximity of the $Al(TfO)_3$ molecule.[92] Thus, the relaxed geometry of $Al(TfO)_3{\cdot}6H_2O$ was constructed, in which six water molecules are located around $Al(TfO)_3$, as shown in Fig. 10(d). Formation of hydrogen bonds

Table 2 Summary of component materials and their properties discussed in this study. All of electrolyte are aqueous based except ref. 86–88

Electrolyte	Anode	Cathode	Initial capacity	Capacity stability	Ref.
5 M of $Al(OTF)_3$	Al	Expanded graphite	10 mAh g^{-1}	50% after 200 cycles	54
5 M of $Al(OTF)_3$	Al	Reduced graphene oxide (rGO)	136 Wh kg^{-1}	60% after 200 cycles	57
5 M $Al(OTF)_3$ and 0.5 M LiOTF	Al	MnO	437 mAh g^{-1}	103 mAh g^{-1} after 100 cycles	62
2 M $Al(OTF)_3$	$Al_{82}Cu_{18}$ alloy	Al_xMnO	400 mAh g^{-1}	83% after 400 cycles	63
5 M of $Al(OTF)_3$	Al	$Al_xMnO_2{\cdot}nH_2O$	481 Wh kg^{-1}	272 mAh g^{-1} after 60 cycles	64
1–5 M of $Al(OTF)_3$	$Al_{82}Cu_{18}$ alloy	Tungsten		Charge/discharge cycling and a current density of 0.2 mA cm^{-2} with voltage gap of 2.6 V	81
1 M of $AlCl_3$	TiO_2	Graphite	62.5 mAh g^{-1}	25 mAh g^{-1} after 1000 cycles	65
1 M of $AlCl_3$	Al	TiO_2	20 mAh g^{-1}	39.5 mAh^{-1} after 20 cycles	66
Poly aluminium ferric chloride	Fe–Al alloy	Nickel hexacyanoferrate (NiFe-PBA)	35 Ah L^{-1}	90% capacity retention after 500 cycles	67
1 M of $AlCl_3$ and KCl	TiO_2	CuHCF (copper-hexacyanoferrate)	15 MWh g^{-1}	70% capacity retention after 1750 cycles	69
2 M of $AlCl_3{\cdot}6H_2O$	Al	Nano graphite	400 mAh g^{-1}	40 mAh g^{-1} at cycle 100	70
4.4 M $AlCl_3$ and 1 M $MnCl_2$ in H_2O	Al	MnO_2	493 mAh g^{-1}	Stable over 1000 cycles	74
1 M of $AlCl_3$	Al	MoO_3	680 mAh g^{-1}	170 mAh g^{-1} after 20th cycle	80
$Al(ClO_4)_3{\cdot}9H_2O$ in succinonitrile to form a hydrated eutectic electrolyte	Al	Polyaniline	185 mAh g^{-1}	Stable over 300 cycles	75
1 M of $Al(NO_3)_3$	Al	Cobalt hexacyanoferrate ($K_2CoFe(CN)_6$)	50 mAh g^{-1}	76% Capacity retention after 1600 cycles	78
1 M of $Al(NO_3)_3$	Polypyrrole coated MoO_3	Copper hexacyanoferrate (CuHCF)		83.2% for 100 cycles	79
2 M of $Al_2(SO_4)_3$	Zn–Al	MnO_2	290 mAh g^{-1}		82
1 M of $Al_2(SO_4)_3$	Ionic Liquid Treated Al	MnO_2	500 Wh kg^{-1}	Stable capacity retention after 40 cycles	83
0.5 M of $Al_2(SO_4)_3$	Amorphous Al	Al_xMnO_2	780 mAh g^{-1}	180 mAh g^{-1} after 80 cycles	84
9 M LiTFSI + 1 M $AlCl_3$	Al	MOF derived N-doped microporous carbon polyhedrons	219.8 mAh g^{-1}		85
$AlCl_3$ and 1 ethyl 3 methylimidazolium chloride (EMIC)	Al	PVP, I_2 and conductve carbon	200 mAh g^{-1}	High stability for over 150 cycles	86
1 M $AlBr_3$ and 0.5 M KBr in ethylbenzene	Al	Glassy carbon	0.4 mAh g^{-1}	Confirmed over 120 cycles	87
0.25 M $Al(PF_6)_3$ in dimethyl sulfoxide	Al	Platinum		Confirmation of Al deposition–stripping	88

between water molecules and the TfO^- ions was also confirmed. The IR spectrum of the relaxed structure of $Al(TfO)_3{\cdot}6H_2O$ based on theoretical calculations is presented in Fig. 10(e) and the wavelength of peaks agree with the experimental spectrum. These results suggest that the interaction between TfO^- ions and Al^{3+} ions did not change when the six solvating water molecules were introduced to $Al(TfO)_3$. They also studied the introduction of $EMIM^+$ and TfO^- ions to $Al(TfO)_3{\cdot}6H_2O$ (data not shown). It was found that AlOH species are formed by deprotonation when water molecules coordinate with Al^{3+} ions. Furthermore, the Al^{3+} solvation environment is changed due to H_3O^+ species from the addition of $EMIM^+$ and TfO^- ions, resulting in altered deposition/stripping behavior of Al.

3.2. Surface treatment

Surface treatment of the Al anode is also a strategy for improvement. As explained above, SEI formation by ILs or deep eutectic solvents could alter the Al anode surface chemistry, yielding stable cell cycling stability even in aqueous electrolytes.[83] Besides ILs, deep eutectic solution can be applied in aluminum anode surface treatment to form SEI.[93] SEI is expected to promote ion transfer, eliminate the passivating oxide layer, create a stable solid protective layer, and improve compatibility between the aqueous electrolyte and the Al anode to stabilize electrochemical performance at the interface. The RAAIB prepared with a surface-treated Al anode, an $FeFe(CN)_6$ cathode, and 2 M $Al(OTF)_3$ as an electrolyte demonstrated a discharge capacity of 85 mAh g^{-1} with a capacity retention of 58 mAh g^{-1} after 150 cycles. Average coulombic efficiency was 97.1% under a 100 mA g^{-1} current density. Since surface treatment is a relatively easy process, it can feasibly be applied industrially for Al-ion battery commercialization.

3.3. Al alloys

Use of aluminum alloys is another effective option to enhance RAAIB performance. Two of the main problems of Al-ion batteries is the oxide layer (Al_2O_3) on the Al anode and side reactions of hydrogen generation. As explained above, a few studies have applied Al–Cu and Zn–Al alloys as anodes for Al-ion batteries.[81] It was also found that the Al–Cu alloy lamellar

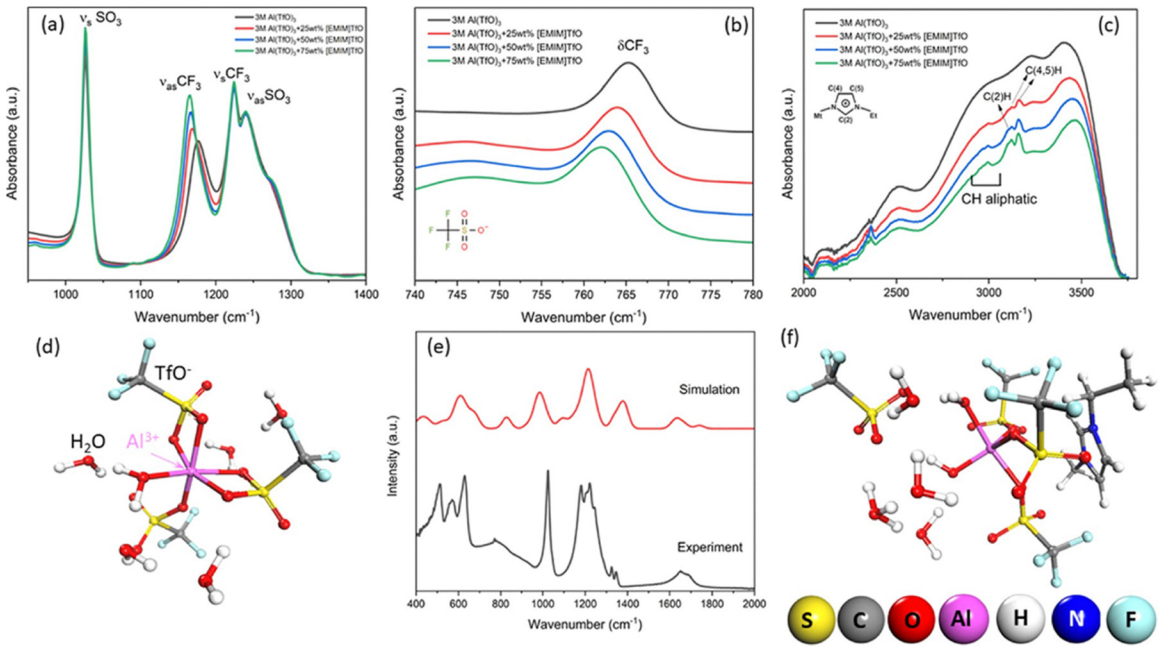

Fig. 10 FT-IR spectra of AlTfO at each concentrations of EMIMTfO. (a) 900 and 1400 cm^{-1}. (b) 740 and 780 cm^{-1}. (c) 2000 and 4000 cm^{-1}. (d) $Al(TfO)_3 \cdot 6H_2O$ Geometries with all the TfO^- ions are being bi-coordinated to the Al^{3+} ion. (e) Comparison of experimental and simulated IR spectra of AlTfO in water. (f) Relaxed geometries of $Al(TfO)_3 \cdot 6H_2O$ with EMIMTfO.

hetero-structures (E-$Al_{82}Cu_{18}$) enhanced Al-ion electrochemical reversibility by achieving dendrite-free Al deposition during redox cycles.[63] Induced by an *in situ* eutectic solidification reaction, E-$Al_{82}Cu_{18}$ possess an aligned lamellar structure consisting of intermetallic Al_2Cu nanolamellas and monometallic α-Al. These two phases pair with each other to give localized galvanic couples of Al/Al_2Cu in periodic structures.

Jia *et al.* studied Sn as an alloying element owing to its good compatibility with Al. They applied a rolling procedure to increase the contact interface area between Al and Sn to create Al–Sn laminate electrodes. This Al–Sn hetero-structure reduced interface resistance and promoted Al stripping/plating.[94] When Al_xMnO_2 cathode was applied, battery delivered a specific capacity of 177 mAh with a stable discharge voltage plateau of 1.5 V. To further ameliorate the electrochemical properties of Al–Sn laminate electrode, a polymer coating was used to reduce HER. Combining this type of anode with a KNHCF cathode, the prepared Al-ion battery maintained 82% capacity retention even after 700 cycles. The author's group also studied the effect of chemical composition of the Al anode especially respect to magnesium impurity, and succeeded in improving the electrochemical performance of RAAIBs.[76]

3.4. Hybrid salts for aqueous electrolytes

A considerable amount of research has been conducted by applying hybrid salt-based electrolytes for other types of metal-ion batteries, including lithium-, zinc-, and magnesium-based batteries.[95–97]

For RAAIBs, a major problem is that the stripping/plating potential of Al^{3+}/Al (−1.68 V) is lower than the hydrogen evolution potential of H^+/H^2. On top of that, the Al anode can be readily corroded under acidic conditions of the aqueous electrolyte. Thus, searching for electrolytes that can solve these issues is essential. Addition of lithium bis(trifluoromethane sulfonyl)imide (LiTFSI) to $AlCl_3$ electrolytes was effective to suppress Al anode corrosion and hydrogen generation. Al-ion batteries with the electrolyte composition of 0.5 M of $AlCl_3$ and 12 M of LiTFSI with a vanadium potassium cathode was prepared, exhibiting 223 mAh g^{-1} at 1000 mA g^{-1} with good stability, maintaining a capacity of 64.6% after 300 cycles.[98] Structural and electrochemical analysis also revealed that a reversible Al^{3+}, Li^+, and H^+ intercalation/de-intercalation reaction occurred in the vanadium potassium cathode during redox reaction.

Gao *et al.* also investigated the effect of an additional second salt to enhance electrochemical performance and to widen the electrochemical window.[99] They attempted a bi-salt aqueous electrolyte based on aluminum-lithium trifluoromethanesulfonate (OTF) dual salt, which resulted in a wide electrochemical window of 4.35 V with a low over-potential of 14.6 mV. $Al_xMnO_2 \cdot nH_2O$ was used as the cathode. It was revealed that the bi-salt electrolyte reduces Mn dissolution, which suppresses self-discharge based on the electrode–electrolyte interface concentrated confinement effect. As a result, the prepared Al-ion battery exhibited a capacity of 364 mAh g^{-1} with a capacity decay rate of 0.37% per cycle over 150 cycles. Furthermore, Yuan *et al.* developed aluminum ammonium hybrid battery with aqueous electrolyte composed of $AlCl_3$ and NH_4Cl and demonstrated 89.3 Wh kg^{-1} capacity with high stability over 10 000 cycles.[100] They have applied prussian blue analogue cathode ($K_{1.14}Fe_{III}[Fe_{II}(CN)_6] \cdot nH_2O$) which demonstrated excellent stability.

Wen *et al.* prepared silicon based inorganic/organic hybrid hydrogel by combining 2 M of $Al(OTF)_3/H_2O$ aqueous solution and TEOS (tetraethyl orthosilicate) by sol–gel polymerization method. With cathode composed of potassium nickel hexacyanoferrate, this hydrogel electrolyte demonstrated a high ionic conductivity of 2.9×10^{-3} S cm^{-1} and delivered initial discharge capacity of 74.9 mAh g^{-1} with capacity retention of 90.0% after 200 cycles.[101]

3.5. Cathode

Another problem that Al ion batteries face is that once Al^{3+} ions are inserted, extracting them from the cathode host is difficult due to strong electrostatic interactions between Al^{3+} ions and the cathode lattice. This irreversible reaction would induce volume expansion and unfavorable structural change. Acidic electrolytes may be necessary to extract Al^{3+} from the cathode, although the acidity would damage and dissolve the cathode's structure. Discussion of cathode choice for aqueous Al-ion batteries can also be accessed in some review studies.[102]

δ-MnO_2 has been reported as a prime candidate for cathode material in aqueous Al-ion batteries owing to its layered crystalline structure combined with large interlayer distance. However, they tend to collapse when high ionic potential multivalent ions such as Al^{3+} intercalates into those layers. In this regard, Chen *et al.* revealed that when heterogeneous metal dopants are introduced into layered crystals, dopants bond to oxygen to make the δ-MnO_2 structure stronger. When δ-MnO_2 is doped with vanadium, the Al-ion battery using 2 M $Al(OTF)_3$ electrolyte demonstrated a specific capacity of 518 mAh g^{-1} at 200 mA g^{-1} with stable cell cycling for 400 cycles (Fig. 11(a)).[103] Electrochemical impedance spectroscopy (EIS) analyses were performed to examine the resistance of δ-MnO_2 cathodes (Fig. 11(b)). Necessary battery resistance values can be obtained by fitting semicircles at the high frequency region and slope lines in the low frequency region, together with the equivalent circuit (Fig. 11(b) inset). R1 in the circuit is the resistance of the electrolyte and R2 is the charge transfer resistance as (R_{ct}). Fig. 11(c) indicates the R_{ct} fitting values, with vanadium-doped δ-MnO_2 cathodes showing the lowest resistance. It was suggested that heterogeneous metal doping in δ-MnO_2 can enhance electrical conductivity and reduce R_{ct} by creating additional pathways for Al^{3+} ion conduction and active sites.[104] Rate capacity performance is shown in Fig. 11(d) and vanadium-doped δ-MnO_2 demonstrated the strongest rate performance even against high current densities. Cycling stability is presented in Fig. 11(e and f), with vanadium-doped δ-MnO_2 delivering the favorable cycling performance at both current densities of 200 and 500 mA g^{-1}.

Besides MnO_2, nanobelt-structured MoO_3 was synthesized by a hydrothermal method and used as a cathode. The high number of active sites of MoO_3 promoted Al^{3+} intercalation/deintercalation reactions and increased the Al^{3+} diffusion rate. This MoO_3 nanobelt cathode-based Al-ion battery displayed 267.61 mAh g^{-1} at 0.2 Ag^{-1} and capacity was maintained even after 100 cycles.[105] Nanostructured Mn_3O_4 has also been applied as cathodes for aqueous Al-ion batteries. Using $AlCl_3$ aqueous electrolytes, Mn_3O_4 cathodes demonstrated 271 mAh g^{-1} under a current density of 0.5 A g^{-1}, yielding a capacity retention of 98% over 1000 cycles.[106] Phase transition from a Mn_3O_4 spinel to a MnO_2-layered structure is hypothesized to be one of the reasons for high cycling stability. The author's group also investigated the potential use of $AlFeO_3$ cathodes, demonstrated high cell performance.[107] There are many cathode candidates besides these materials such as carbon, graphite, and sulfur, which should be discussed in a forthcoming paper.

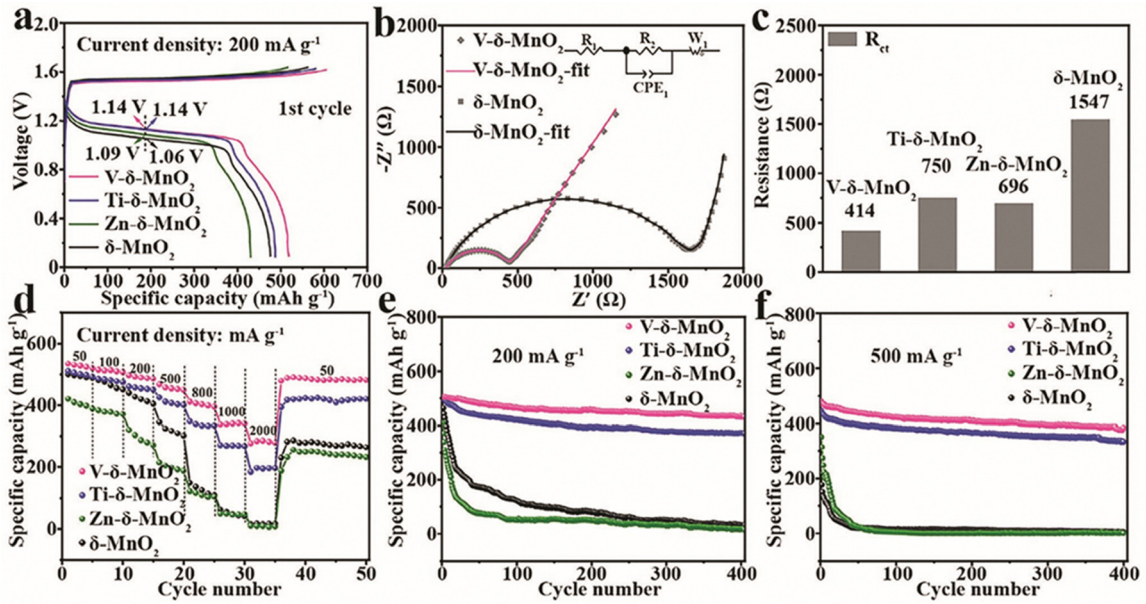

Fig. 11 Various electrochemical measurements of intact and doped δ-MnO_2 cathodes. (a) 1st charge–discharge curves at a current density of 200 mg^{-1}. (b) Cole–Cole plots of V-δ-MnO_2 and δ-MnO_2 electrodes (Inset presents the equivalent circuit). (c) The charge transfer resistance of intact and doped δ-MnO_2 cathodes. (d) Rate performances of each δ-MnO_2 cathodes. (e) and (f) Cycling performances under 200 and 500 mA g^{-1}, respectively.

4. Conclusion and future prospects

As explained above, numerous studies have taken on the challenge to overcome the major obstacles of RAAIBs, which includes Al anode corrosion, dendrite formation, and passivation of the inert Al_2O_3 layer. Intercalation/de-intercalation of Al^{3+} ions from the cathode material is also a major problem for RAAIBs. So far, aluminum chloride- and fluoride-based aqueous electrolytes seem to be the most promising. Furthermore, addition of ILs, deep eutectic solvents into water-based electrolytes, surface treatment of aluminum anodes, alloying of aluminum anodes, hybrid salt application, and cathode optimization are all necessary directions for future research topics to make RAAIBs feasible for industrial rechargeable batteries.

Conflicts of interest

There are no conflicts to declare.

Data availability

No new data were created or analyzed in this study. This review is based on existing literatures and previously published datasets, as cited in the reference list.

Acknowledgements

The author wishes to express thanks to Dr. Hideki Yoshioka, Ms. Maiko Mori and Ms. Ayako Mori for their helpful discussions.

References

1 S. Orangi, N. Manjong, D. P. Clos, L. Usai, O. S. Burheim and A. H. Strømman, *J. Energy Storage*, 2024, **76**, 109800–109813.
2 W. Q. Chen, *J. Ind. Ecol.*, 2013, **17**, 926–938.
3 R. Mori, *RSC Adv.*, 2017, **7**, 6389–6395.
4 R. Mori, *Sustainable Energy Fuels*, 2017, **1**, 1082–1089.
5 R. Mori, *Phys. Chem. Chem. Phys.*, 2018, **20**, 29983–29988.
6 Q. Liu, H. Wang, C. Jiang and Y. Tang, *Energy Storage Mater.*, 2019, **23**, 566–586.
7 M. H. Alfaruqi, S. Islam, J. Lee, J. Jo, V. Mathew and J. Kim, *J. Mater. Chem. A*, 2019, **7**, 26966–26974.
8 A. M. Diem, J. Bill and Z. Burghard, *ACS Appl. Energy Mater.*, 2020, **3**, 4033–4042.
9 S. Wang, *et al.*, *ACS Appl. Nano Mater.*, 2019, **2**, 6428–6435.
10 J. Tu, H. Lei, Z. Yu and S. Jiao, *Chem. Commun.*, 2018, **54**, 1343–1346.
11 H. Li, H. Yang, Z. Sun, Y. Shi, H.-M. Cheng and F. Li, *Nano Energy*, 2019, **56**, 100–108.
12 S. Guo, H. Yang, M. Liu, X. Feng, H. Xu, Y. Bai and C. Wu, *ACS Appl. Energy Mater.*, 2021, **4**, 7064–7072.
13 S. Liu, G. L. Pan, G. R. Li and X. P. Gao, *J. Mater. Chem. A*, 2015, **3**, 959–962.
14 K. Q. Qin, J. H. Huang, K. Holguin and C. Luo, *Energy Environ. Sci.*, 2020, **13**, 3950–3992.
15 S. Wang, S. Huang, M. Yao, Y. Zhang and Z. Niu, *Angew. Chem., Int. Ed.*, 2020, **59**, 11800–11807.
16 P. R. Gifford and J. B. Palmisano, *J. Electrochem. Soc.*, 1987, **134**, 610–614.
17 X. Z. Yu, B. Wang, D. C. Gong, Z. Xu and B. G. Lu, *Adv. Mater.*, 2017, **29**, 1604118.
18 E. Zhang, J. Wang, B. Wang, X. Yu, H. Yang and B. Lu, *Energy Storage Mater.*, 2019, **23**, 72–78.
19 J. Zhang, R. He, L. Jia, C. You, Y. Zhang, M. Liu, N. Tian, H. Lin and J. Wang, *Adv. Funct. Mater.*, 2023, **33**, 2305674.
20 S. Licht and D. Peramunage, *J. Electrochem. Soc.*, 1993, **140**, L4–L7.
21 J. Zhao, *et al.*, *Green Chem.*, 2025, **27**, 352.
22 C. Yan, *et al.*, *J. Am. Chem. Soc.*, 2022, **144**, 11444–11455.
23 S. Peng, *et al.*, *ACS Sustainable Chem. Eng.*, 2021, **9**, 3710–3717.
24 Q. Ran, S. P. Zeng, M. H. Zhu, W. B. Wan, H. Meng, H. Shi, Z. Wen, X. Y. Lang and Q. Jiang, *Adv. Funct. Mater.*, 2022, **33**, 2211271.
25 E. Zemlyanushin, B. Schwarz and S. Dsoke, *J. Power Sources*, 2025, **633**(30), 236458.
26 M. Angell, C. J. Pan, Y. Rong, C. Yuan, M. C. Lin, B. J. Hwang and H. Dai, *Proc. Natl. Acad. Sci. U. S. A.*, 2017, **114**(5), 834–839.
27 G. A. Elia, O. B. Ducros, D. Sotta, V. Delhorbe, A. Brun, K. Marquardt and R. Hahn, *ACS Appl. Mater. Interfaces*, 2017, **9**(44), 38381–38389.
28 Y. Liu, *et al.*, *Nano Energy*, 2024, **130**, 110140.
29 P. Meng, Z. Yang, J. Zhang, M. Jiang, Y. Wang, X. Zhang, J. Luo and C. Fu, *Energy Storage Mater.*, 2023, **63**, 102953.
30 J. Verma and D. Kumar, *Nanoscale Adv.*, 2021, **3**, 3384.
31 Y. Guo, F. Sun, T. Zhu, C. Zhang, K. Feng, X. Wang, G. Feng, F. You and C. Liang, *Electrochim. Acta*, 2024, **507**(10), 145196.
32 E. O. Filatova and A. S. Konashuk, *J. Phys. Chem. C*, 2015, **119**, 20755–20761.
33 J. S. Wilkes, J. A. Levisky, R. A. Wilson and C. L. Hussey, *Inorg. Chem.*, 1982, **21**, 1263–1264.
34 J. Smajic, S. Wee, F. R. F. Simoes, M. N. Hedhili, N. Wehbe, E. Abou-Hamad and P. M. F. J. Costa, *ACS Appl. Energy Mater.*, 2020, **3**, 6805–6814.
35 D. Y. Wang, *et al.*, *Nat. Commun.*, 2017, **8**, 14283.
36 M. Angell, C. J. Pan, Y. Rong, C. Yuan, M. C. Lin, B. J. Hwang and H. Dai, *Proc. Natl. Acad. Sci. U. S. A.*, 2017, **114**(5), 834–839.
37 Z. Zhang, A. Kitada, S. Gao, K. Fukami, N. Tsuji, Z. Yao and K. Murase, *ACS Appl. Mater. Interfaces*, 2020, **12**, 43289–43298.
38 K. V. Kravchyk and M. V. Kovalenko, *Commun. Chem.*, 2020, **3**, 120.
39 C. Xie, *et al.*, *Adv. Funct. Mater.*, 2024, **34**(48), 2408296.
40 Z. Yuan, Q. Lin, Y. Li, W. Han and L. Wang, *Adv. Mater.*, 2023, **35**(17), 2211527.
41 H. Wang, *et al.*, *Energy Environ. Sci.*, 2022, **15**(1), 311.
42 E. Faegh, B. Ng, D. Hayman and W. E. Mustain, *Nat. Energy*, 2021, **6**(1), 21.

43 C. Xu, T. Diemant, X. Liu and S. Passerini, *Adv. Mater.*, 2024, **36**(24), 2400263.
44 C. Wang, J. Li, H. Jiao, J. Tu and S. Jiao, *RSC Adv.*, 2017, **7**, 32288–32292.
45 X. Shen, *et al.*, *Nat. Commun.*, 2021, **12**, 820–831.
46 L. D. Reed, S. N. Ortiz, M. Xiong and E. J. Menke, *Chem. Commun.*, 2015, **51**, 14397–14400.
47 A. Mohammad, T. Köhler, S. B. H. Stöcker and D. C. Meyer, *ACS Appl. Energy Mater.*, 2023, **6**(5), 2914–2923.
48 Z. Yu, Y. Xie, W. Wang, J. Hong and J. Ge, *Front. Chem.*, 2023, **11**, 1190102.
49 J. Smajicz and P. M. F. J. Costa, *J. Electrochem. Soc.*, 2022, **169**, 040549.
50 W. Tang, L. Deng, L. Guo, S. Zhou, Q. Jiang and J. Luo, *Green Energy Environ.*, 2024, **9**, 1183–1191.
51 J. Vatamanu and O. Borodin, *J. Phys. Chem. Lett.*, 2017, **8**, 4362–4367.
52 Y. Li, L. Liu, Y. Lu, R. Shi, Y. Ma, Z. Yan, K. Zhang and J. Chen, *Adv. Funct. Mater.*, 2021, **31**, 2102063.
53 J. F. Stoddart, D. J. Kim, J. W. Choi and D. J. Yoo, *Angew. Chem., Int. Ed.*, 2021, **60**, 5794.
54 J. Smajic, A. Alazmi, N. Wehbe and P. M. F. J. Costa, *Nanomaterials*, 2021, **11**, 3235–3244.
55 L. N. Xu, J. Y. Zhu, M. X. Lu, L. Zhang and W. Chang, *Int. J. Miner., Metall. Mater.*, 2015, **22**, 500–508.
56 B. A. Boukamp, *Solid State Ionics*, 2001, **143**, 47–55.
57 M. F. J. Costa, *Adv. Mater. Interfaces*, 2021, 2101733.
58 C. D. Wagner, A. V. Naumkin, A. Kraut-Vass, J. W. Allison, C. J. Powell and J. R. Rumble Jr., NIST standard reference database, National Institute of Standards and Technology, Gaithersburg, Maryland, USA 2003.
59 J. Chen, Q. Zhu, L. Jiang, R. Liu, Y. Yang, M. Tang, J. Wang, H. Wang and L. Guo, *Angew. Chem.*, 2021, **60**, 5794.
60 B. Wang, A. J. Fielding and R. A. Dryfe, *J. Phys. Chem. A*, 2019, **123**, 22556.
61 M. J. Park, H. Y. Asl and A. Manthiram, *ACS Energy Lett.*, 2020, **5**, 2367.
62 Q. Sun, L. Chai, S. Chen, W. Zhang, H. Y. Yang and Z. Li, *ACS Appl. Mater. Interfaces*, 2024, **16**(8), 10061–10069.
63 Q. Ran, *et al.*, *Nat. Commun.*, 2022, **13**, 576.
64 C. Wu, *et al.*, *Nat. Commun.*, 2019, **10**, 73.
65 S. Nandi, H. Lahan and S. K. Das, *Bull. Mater. Sci.*, 2020, **43**, 26.
66 B. Unal, O. Sel and R. D. Cakan, *J. Appl. Electrochem.*, 2024, **54**, 1425.
67 R. Tao, C. Gao, E. Xie, B. Wang and B. Lu, *Chem. Sci.*, 2022, **13**, 10066.
68 C. Gao, *et al.*, *Adv. Funct. Mater.*, 2018, **28**, 1803129.
69 A. Holland, R. D. Mckerracher, A. Cruden and R. G. A. Wills, *et al.*, *J. Appl. Electrochem.*, 2018, **48**, 243.
70 S. A. Rastabi, G. Razaz, M. Hummelgård, T. Carlberg, N. Blomquist, J. Ortegren and H. Olin, *J. Power Sources*, 2022, **523**, 231066.
71 J. R. Davis, *ASM International Handbook*, 1993, p. 547.
72 G. Razaz and T. Carlberg, *Metall. Mater. Trans.*, 2019, **A50**(4), 1873.
73 Y. J. Cho, I. J. Park, H. J. Lee and J. G. Kim, *J. Power Sources*, 2015, **277**, 370.
74 Y. Xu, *et al.*, *Energy Storage Mater.*, 2022, **47**, 113.
75 P. Meng, J. Huang, Z. Yang, F. Wang, T. Lv, J. Zhang, C. Fu and W. Xiao, *Adv. Mater.*, 2022, **34**(8), 2106511.
76 R. Mori, Japan Patent Application Number, 2025-055734.
77 R. Mori, Japan Patent Application Number, 2025-055735.
78 Y. Ru, S. Zheng, H. Xue and H. Pang, *Chem. Eng. J.*, 2020, **382**, 122853.
79 P. Wang, *et al.*, *Chem. Eng. J.*, 2019, **373**, 580.
80 H. Lahan and S. K. Das, *J. Power Sources*, 2019, **413**, 134.
81 Y. H. Wu, W. J. Lin, T. H. Tsai and M. C. Lin, *ACS Appl. Energy Mater.*, 2024, **7**, 3957.
82 A. Ejigu, L. W. Le Fevre, A. Elgendy, B. F. Spencer, C. Bawn and R. A. W. Dryfe, *ACS Appl. Mater. Interfaces*, 2022, **14**, 25232.
83 Q. Zhao, M. J. Zachman, W. I. A. Sadat, J. Zheng, L. F. Kourkoutis and L. Archer, *Sci. Adv.*, 2018, **4**, eaau8131.
84 Y. Chunshuang, *et al.*, *J. Am. Chem. Soc.*, 2022, **144**(25), 11444.
85 S. Yang, C. Li, H. Lv, X. Guo, Y. Wang, C. Han, C. Zhi and H. Li, *Small Methods*, 2021, **5**(10), 2100611.
86 H. Tian, S. Zhang, Z. Meng, W. He and W. Q. Han, *ACS Energy Lett.*, 2017, **2**(5), 1170.
87 M. Chiku, H. akeda, Y. Yamaguchi, E. Higuchi and H. Inoue, *Int. J. Chem.*, 2013, **5**, 4.
88 X. Wen, *et al.*, *J. Phys. Chem. Lett.*, 2021, **12**(25), 5903.
89 A. Lahiri, S. Guan and A. Chutia, *ACS Appl. Energy Mater.*, 2023, **6**, 11874.
90 V. Balland, M. Mateos, A. Singh, K. D. Harris, C. L. Robust and B. Limoges, *Small*, 2021, **17**, 2101515.
91 P. A. Parayad, *et al.*, *Eur. J. Inorg. Chem.*, 2018, 14146.
92 G. R. Pastel, *et al.*, *Energy Environ. Sci.*, 2022, **15**, 2460.
93 R. Bai, J. Yang, G. Li, J. Luo and W. Tang, *Energy Storage Mater.*, 2021, **41**, 41.
94 B. E. Jia, *et al.*, *Energy Storage Mater.*, 2024, **65**, 103141.
95 F. Wang, O. Borodin, T. Gao, X. Fan, W. Sun and F. Han, *et al.*, *Nat. Mater.*, 2018, **17**, 543.
96 L. Suo, *et al.*, *Angew. Chem., Int. Ed.*, 2016, **55**, 7136.
97 T. Yang, *et al.*, *Appl. Surf. Sci.*, 2024, **660**, 159995.
98 X. Li, *et al.*, *J. Mater. Chem. A*, 2022, **10**, 4739.
99 Y. Gao, Y. Li, H. Yang, L. Zheng, Y. Bai and C. Wu, *J. Energy Chem.*, 2022, **67**, 613.
100 X. Yuan, *et al.*, *Adv. Energy Mater.*, 2025, **15**, 16.
101 Z. Wen, *et al.*, *Adv. Mater.*, 2025, **37**(15), 2500695.
102 H. Yang, H. Li, J. Li, Z. Sun, K. He, H. M. Cheng and F. Li, *Angew. Chem., Int. Ed.*, 2019, **58**, 11978.
103 S. Chen, Y. Kong, C. Tang, N. A. Gadelhak, A. K. Nanjundan, A. Du, C. Yu and X. Huang, *Small*, 2024, **20**, 2312229.
104 J. L. Yang, W. B. Gong and F. X. Geng, *Adv. Funct. Mater.*, 2023, **33**, 2301202.
105 L. Chen, C. Lv, H. Gu, W. Zhang and Z. Li, *J. Colloid Interface Sci.*, 2025, **677**, 1045.
106 P. De, L. Bharti, J. Halder, S. Priya and A. Chandra, *Electrochim. Acta*, 2023, **469**(20), 143248.
107 R. Mori, Japan Patent Application Number, 2025- 008535.